Polarization-Sensitive Optical Coherence Tomographic Documentation of Choroidal Melanin Loss in Chronic Vogt–Koyanagi–Harada Disease

Masahiro Miura,[1,2] Shuichi Makita,[3] Yoshiaki Yasuno,[3] Rintaro Tsukahara,[1,2] Yoshihiko Usui,[2] Narsing A. Rao,[4] Yasushi Ikuno,[5] Sato Uematsu,[6] Tetsuya Agawa,[2] Takuya Iwasaki,[1,2] and Hiroshi Goto[2]

[1]Department of Ophthalmology, Tokyo Medical University, Ibaraki Medical Center, Ami, Japan
[2]Department of Ophthalmology, Tokyo Medical University, Tokyo, Japan
[3]Computational Optics Group, University of Tsukuba, Tsukuba, Japan
[4]USC-Roski Eye Institute, University of Southern California, Los Angeles, California, United States
[5]Ikuno Eye Center, Osaka, Japan
[6]Department of Ophthalmology, Osaka University Graduate School of Medicine, Suita, Japan

Correspondence: Masahiro Miura, Department of Ophthalmology, Tokyo Medical University, Ibaraki Medical Center, 3-20-1 Chuo, Ami, Inashiki, Ibaraki 300395, Japan; m-miura@tokyo-med.ac.jp.

Submitted: April 25, 2016
Accepted: August 1, 2017

Citation: Miura M, Makita S, Yasuno Y, et al. Polarization-sensitive optical coherence tomographic documentation of choroidal melanin loss in chronic Vogt–Koyanagi–Harada disease. *Invest Ophthalmol Vis Sci*. 2017;58:4467–4476. DOI:10.1167/iovs.17-22117

Purpose. Vogt–Koyanagi–Harada (VKH) disease is a systemic autoimmune disorder that affects organs with melanocytes. The sunset glow fundus (SGF) in VKH disease was evaluated with polarization-sensitive optical coherence tomography (PS-OCT).

Methods. The study involved 28 eyes from 14 patients with chronic VKH disease, 21 eyes from 21 age-matched controls, and 22 eyes from 22 high-myopic patients with a tessellated fundus. VKH eyes were grouped into sunset or non-sunset groups on the basis of color fundus images. The presence of melanin in the choroid was determined by using the degree of polarization uniformity (DOPU) obtained by PS-OCT. The sunset glow index (SGI) was calculated by using color fundus images. Presence of an SGF was evaluated by using DOPU, SGI, subfoveal choroidal thicknesses, near-infrared images, and autofluorescence images at 488 nm (SW-AF) and 785 nm (NIR-AF).

Results. There were 16 eyes in the sunset group and 12 eyes in the non-sunset group. For all eyes in the sunset group, the disappearance of choroidal melanin was clearly detected with PS-OCT. Percentage areas of low DOPU in the choroidal interstitial stroma of the sunset group were significantly lower than those of other groups and showed no overlap with other groups. The distribution of choroidal thicknesses and SGI in the sunset group substantially overlapped with other groups. The subjective analyses of the sunset and non-sunset groups, using near infrared, SW-AF, or NIR-AF, showed substantial inconsistencies with the PS-OCT results.

Conclusions. PS-OCT provides an in vivo objective evaluation of choroidal melanin loss of the SGF in chronic VKH disease.

Keywords: polarization, melanocyte, Vogt-Koyanagi-Harada disease, optical coherence tomography

Vogt–Koyanagi–Harada (VKH) disease is a systemic autoimmune disorder that affects organs with melanocytes, including the eye, meninges, skin, and inner ear.[1] The clinical course of VKH disease follows four phases: prodromal, uveitis, convalescent, and recurrent/chronic.[1] In the convalescent or recurrent/chronic stage, depigmentation of the choroid results from choroidal melanocyte damage[2,3] and the fundus shows bright orange discoloration. This clinical finding is known as a "sunset glow fundus" (SGF).[1]

SGF is highly specific to VKH disease and is identified as an important finding in the Revised Diagnostic Criteria of VKH disease.[4] An association of SGF appearance with the severity of meningitis and chronic ocular inflammation has been reported.[5,6] In some cases, changes in an SGF develop a few years after onset of VKH disease, without clinically significant intraocular inflammatory findings.[7,8] This delayed development is considered to result from the persistence of subclinical choroidal inflammation. SGF represents the natural course of VKH resulting from insufficient treatment, so accurate diagnosis of an SGF is important for the clinical management of this disorder.

Diagnosis of an SGF is usually based on subjective evaluation of color fundus (CF) images.[9] Given this subjective evaluation, "sunset glow fundus" is a descriptive and somewhat subjective clinical term, despite its clinical importance, and this uncertainty can cause difficulty in diagnosing an SGF.[10] SGF might be confounded with the normally hypopigmented fundus of some Caucasian individuals.[9] Suzuki[7] has proposed the use of the sunset glow index (SGI), involving an objective evaluation of color balance in scanned CF images and reported its usefulness in evaluating the severity of the SGF. However, a lack of further research meant this method was rarely used in clinical studies

Table. Summary of Patients With Vogt–Koyanagi–Harada Disease

Case	Sex	Age, y	Classification with CF	Duration, mo	Phase in VKH Disease	Initial Therapy
1	F	82	Non-sunset	15	Convalescent phase	BTM 8 mg × 7 d
2	F	82	Non-sunset	19	Convalescent phase	BTM 6 mg × 3 d
3	F	69	Non-sunset	35	Chronic/recurrence phase	BTM 8 mg × 13 d
4	M	39	Non-sunset	39	Convalescent phase	BTM 8 mg × 8 d
5	F	52	Non-sunset	42	Convalescent phase	BTM 8 mg × 7 d
6	F	45	Non-sunset	52	Convalescent phase	BTM 10 mg × 7 d
7	M	45	Sunset	13	Chronic/recurrence phase	BTM 8 mg × 9 d
8	M	53	Sunset	14	Convalescent phase	BTM 8 mg × 8 d
9	M	65	Sunset	17	Convalescent phase	BTM 8 mg × 8 d
10	M	62	Sunset	24	Convalescent phase	BTM 8 mg × 8 d
11	M	44	Sunset	27	Chronic/recurrence phase	BTM 8 mg × 7 d
12	M	75	Sunset	60	Convalescent phase	BTM 8 mg × 7 d
13	M	56	Sunset	132	Chronic/recurrence phase	Unknown
14	F	81	Sunset	300	Chronic/recurrence phase	Unknown

BTM, betamethasone; F, female; M, male.

of VKH disease. Another possible diagnostic method involves choroidal thickness measurements. Some studies show a decrease in choroidal thickness with an SGF,[11,12] but these studies do not correlate the extent and severity of SGF appearance with choroidal thickness.

Polarization-sensitive optical coherence tomography (PS-OCT) is a functional extension of OCT technology that uses the polarization properties to acquire three-dimensional (3D) retinal and choroidal information.[13] Multiple scattered light from melanin in tissue induces depolarization, which is found in melanin-containing structures such as the retinal pigment epithelium (RPE) and choroidal melanocytes.[14–16] PS-OCT provides 3D information about melanin distribution in the retina and choroid and might be useful for the objective evaluation of the disappearance of choroidal melanocytes in an SGF. In this study, we evaluated the pathologic condition of choroidal melanocytes in an SGF by using PS-OCT and compared the PS-OCT findings with other multimodal imaging modalities.

Methods

Participants

This cross-sectional study was performed according to the tenets of the Declaration of Helsinki. This study was approved by the institutional review board of Tokyo Medical University and was registered in a public database (UMIN000026307; http://www.umin.ac.jp/ctr/index-j.htm). The nature of the current study and the implications of participating in this research were explained to all study candidates and written informed consent was obtained from each participant before any study procedures or examinations were performed. Eyes with severe cataract or other eye diseases that could compromise the image quality were excluded.

We examined 28 eyes from 14 Japanese patients (8 males, 6 females; age range, 39–82 years; mean age, 60.7 years) with a chronic stage of VKH disease (Table). The diagnosis of VKH disease was based on the revised criteria proposed by the International Nomenclature Committee.[4] Mean duration from the initial onset was 56.4 months (range, 13–300 months). Among the patient cohort, 10 eyes from five patients were in the remission period of the chronic/recurrence phase and another 18 eyes from nine patients were in the convalescent phase without recurrence. Twelve participants were initially treated with 6 to 10 mg intravenous betamethasone for 3 to 13 days followed by oral prednisolone. For two other patients (Table, cases 13 and 14), exact dosages and durations of initial therapies were not available because these patients were referred to our institute for further follow-up. Two eyes from one patient (Table, case 14) received cataract surgery with intraocular lens implantation. The mean spherical equivalent refractive error was −2.1 diopters (D) (range, −7.0 to +0.25 D). The mean axial length was 24.2 mm (range, 23.0–26.3 mm).

For the age-matched control group, we evaluated 21 eyes from 21 healthy Japanese participants (17 males, 4 females; age range, 30–88 years; mean age, 57.0 years). Exclusion criteria for the control group were a history of intraocular surgery, retinal and or choroidal pathology, or glaucoma. The ages of the control group were not significantly different from those of the VKH disease patients ($P = 0.53$; Mann-Whitney U test). In the control group, the right eye was evaluated in 17 participants and the left eye was evaluated in 4 participants. The mean spherical equivalent refractive error was −2.5 D (range, −7.50 to +2.25 D). The mean axial length was 24.5 mm (range, 23.1–26.5 mm).

We evaluated 22 eyes from 22 Japanese patients with high myopia and tessellated fundus (4 males, 18 females; age range, 18–77 years; mean age, 54.2 years [tessellated fundus group]). In this group, the right eye was evaluated in 10 patients and the left eye was evaluated in 12 patients. Seven eyes received cataract surgery with intraocular lens implantation. The mean axial length was 29.9 mm (range, 27.1–33.3 mm) and the mean spherical equivalent refractive error was −11.9 D (range, −3.0 to −25.5 D). The ages of the high-myopia group were not significantly different from those of patients with VKH disease ($P = 0.43$; Mann-Whitney U test).

Polarization-Sensitive Optical Coherence Tomography Imaging

A detailed description of the prototype PS-OCT system, built by the Computational Optic Group at the University of Tsukuba, has been previously reported.[17,18] This PS-OCT system is a multifunctional Jones-matrix OCT, using a swept-source laser with a central wavelength of 1048 nm. The depth range of each B-scan image was 2.1 mm and the depth resolution in tissue was 6.6 μm. The axial scan speed was 100,000 A-scans/s. A raster scanning protocol with 512 A-lines × 256 B-scans covering a 6.0 × 6.0-mm region on the retina was used for volumetric scans and the acquisition speed of each volumetric measurement was 6.6 s/vol. For the PS-OCT measurements, B-scan measurements were repeated four times at a single location. The degree of polarization uniformity (DOPU) was

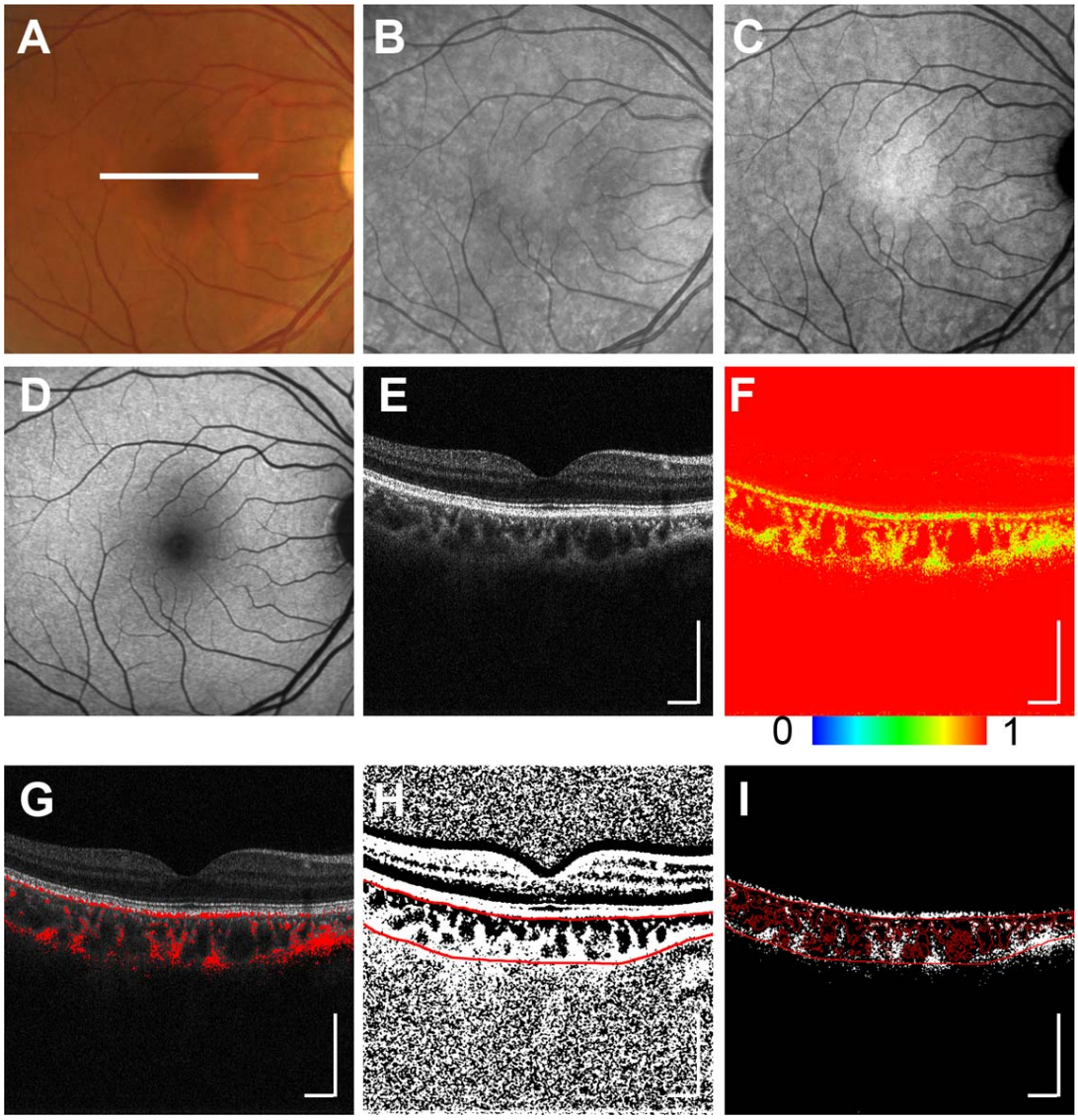

FIGURE 1. Multimodal imaging of the right eye of a 54-year-old female from the control group. The *white line* in the CF image (**A**) designates the scan line of the PS-OCT B-scan image (**E**–**I**). Neither the NIR image (**B**), NIR-AF image (**C**), SW-AF image (**D**), nor standard OCT B-scan image (**E**) provides information about the melanin density in the choroid. The DOPU B-scan image (**F**) and composite DOPU B-scan OCT image (**G**) show the melanin distribution in the RPE and choroid. Binarization was applied for the standard OCT B-scan image to detect the choroidal interstitial area (**H**) and *red lines* indicate manually segmented lines of the choroid (**H**). The *red lines* in the B-scan image for the calculation of percentage area of low DOPU (**I**) show the boundary of the choroidal interstitial stroma. The *scale bar* in B-scan images represents 500 μm × 500 μm.

calculated to evaluate the depolarization or the polarization scramble of the tissue.[19] In our analyses, the DOPU with Makita's noise correction was computed by using a 3 pixel (transverse) × 3 pixel (depth) kernel.[20] Composite DOPU B-scan OCT images, in which the area of low DOPU (<0.8) was overlaid on the standard OCT B-scan image with red color, were created to specify the location of the depolarization observed in the standard OCT image (Figs. 1G, 2G, 3G, 4D). Standard B-scan OCT images were calculated by averaging four sets of PS-OCT B-scan images.

For the objective evaluation of choroidal melanin, we calculated the percentage area of low DOPU in the choroidal interstitial stroma. First, the choroid area in the standard OCT B-scan images was manually selected by a retina specialist (MM). Binarization using the local Otsu method, followed by median filtering, was applied for the standard OCT B-scan images by using image processing software (Fiji[21]) to separate the choroidal area into vessel and interstitial area (Figs. 1H, 2H, 3H, 4E). The percentage area of low DOPU (<0.8), which is the occupancy of the low DOPU area within the choroidal interstitial stroma, was calculated from the B-scan DOPU images (Figs. 1I, 2I, 3I, 4F). For each eye, the percentage area of low DOPU was calculated by using the mean of three horizontal B-scan images (e.g., foveal B-scan, 3 mm above the fovea and 3 mm below the fovea; Fig. 5). To determine the repeatability, we evaluated the percentage area of low DOPU for 10 eyes from 10 participants in the control group (9 males, 1 female; age range, 30–69 years; mean age, 47.9 years; 8 right eyes and 2 left eyes). The coefficient of variation was calculated by four repeated measurements for each participant.

Multimodal Imaging

For multimodal imaging, near-infrared (NIR; 817 nm) images, near-infrared autofluorescence (NIR-AF; 785 nm excitation,

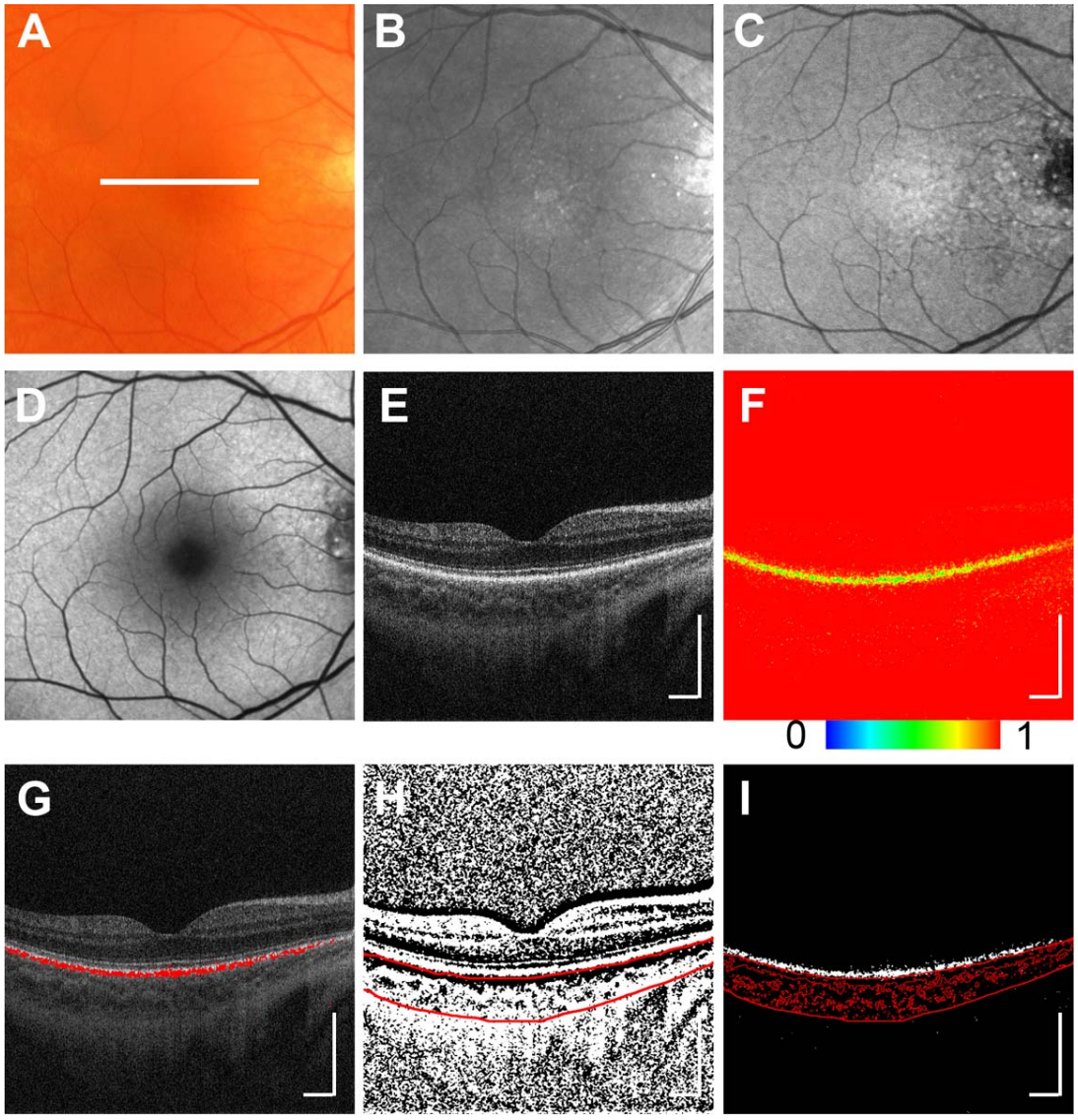

FIGURE 2. Multimodal imaging from the right eye of a 45-year-old male (case 7) from the sunset group. The *white line* in the CF image (**A**) indicates the scan line of the PS-OCT B-scan image (**E**–**I**). Neither the NIR image (**B**), NIR-AF image (**C**), SW-AF image (**D**), nor standard OCT B-scan image (**E**) provides information about melanin density in the choroid. The DOPU B-scan image (**F**) and composite DOPU B-scan OCT image (**G**) show the disappearance of choroidal melanin. The *red lines* in the binary image indicate the segmentation line of the choroid (**H**). The *red lines* in the B-scan image for the calculation of percentage area of low DOPU (**I**) show the boundary of the choroidal interstitial stroma. The *scale bar* in B-scan images represents 500 μm × 500 μm.

emission > 800 nm) images, and short-wavelength autofluorescence (SW-AF; 488 nm excitation, emission > 500 nm) images were obtained with the confocal scanning laser ophthalmoscope (HRA2; Heidelberg Engineering, Heidelberg, Germany). Square images with side lengths of 30° (768 pixels) were saved in an 8-bit grayscale. CF images with a 50° (1100 pixels) visual angle were captured with a Topcon TRC50IX retinal camera (Topcon, Tokyo, Japan). From captured CF images, square images with side lengths of 30° (660 pixels) around the fovea were clipped for subjective evaluation (Fig. 5). Using CF, NIR, NIR-AF, and SW-AF images, each eye was individually evaluated by two blinded observers (RT, TA) in terms of the presence of an SGF. In the case of discrepancies, a third observer (TI) acted as a referee and helped reach a consensus. From subjective evaluations with CF images, the eyes with VKH disease were classified by the presence (sunset group) or absence (non-sunset group) of the SGF.

For the objective evaluation of the color balance in the CF images without optic disc or peripapillary atrophy, square images with side lengths of 300 pixels were prepared. According to the image analysis software (IMAGEnet; Topcon), this equated to approximately 6 mm around the fovea (Fig. 5). Three-color channel luminance histograms on a 256-step scale were measured with image processing software (Fiji[21]). In this study, we calculated the SGI in the same mean with previous studies as follows[7,22,23]:

$$SGI = L_{red}/(L_{red} + L_{green} + L_{blue}),$$

where L_{red} was the mean luminance of the red channel, L_{green} was the mean luminance of the green channel, and L_{blue} was the mean luminance of blue channel. The SGI was calculated for eyes in the sunset, non-sunset, control, and tessellated fundus groups.

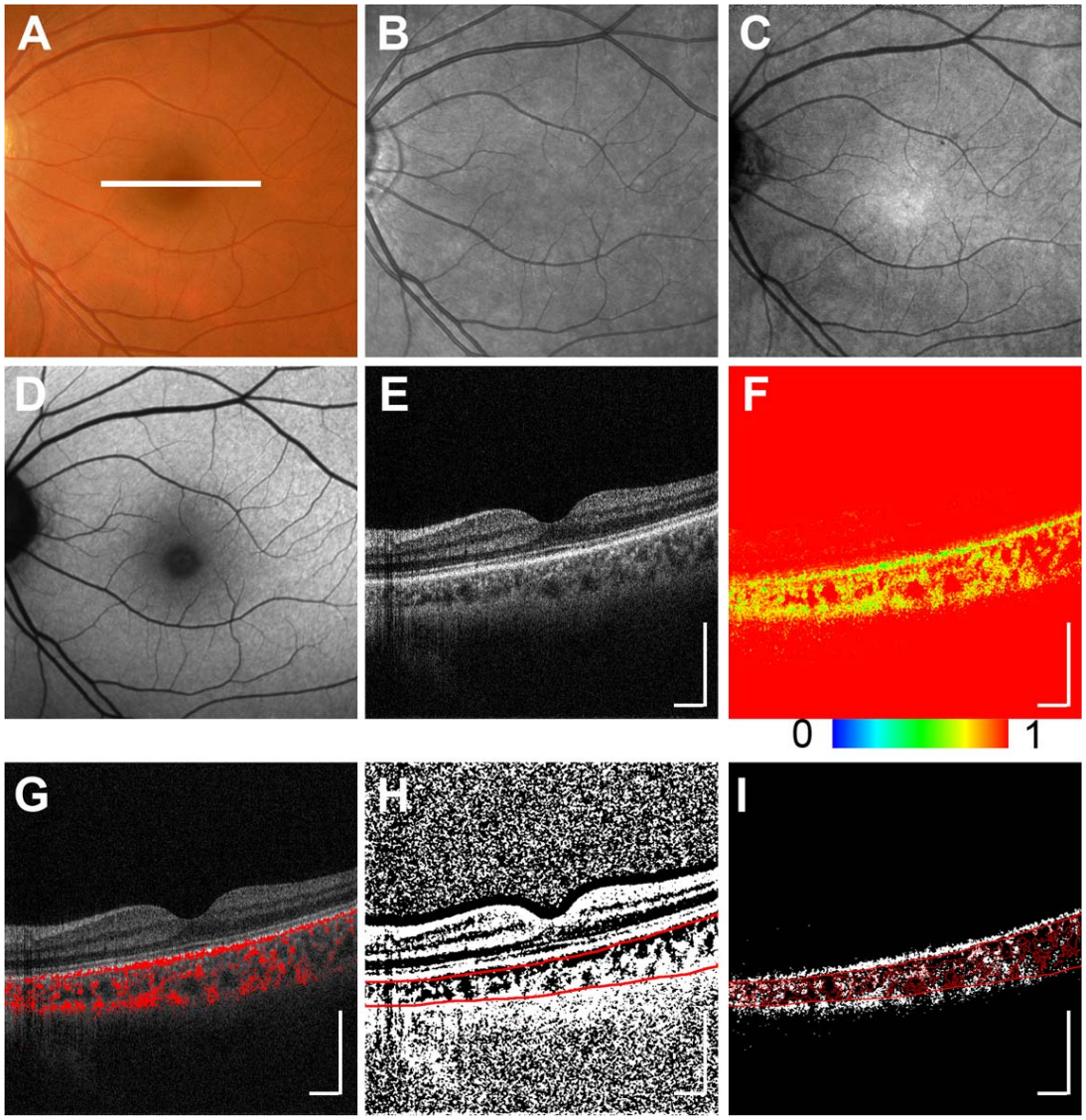

FIGURE 3. Multimodal imaging from the left eye of a 45-year-old female (case 6) from the non-sunset group. The *white line* in the CF image (**A**) indicates the scan line of the PS-OCT B-scan image (**E**–**I**). Neither the NIR image (**B**), NIR-AF image (**C**), SW-AF image (**D**), nor standard OCT B-scan image (**E**) provides information about melanin density in the choroid. The DOPU B-scan image (**F**) and composite DOPU B-scan OCT image (**G**) show the melanin distribution in the RPE and choroid. The *red lines* in the binary image indicate the segmentation line of the choroid (**H**). The *red lines* in the B-scan image for the calculation of the percentage area of low DOPU (**I**) show the boundary of the choroidal interstitial stroma. The *scale bar* in B-scan images represents 500 μm × 500 μm.

For subfoveal choroidal thickness measurements, the choroid area in standard OCT B-scan images was defined as the layer between the RPE and the choroidoscleral interface in standard OCT B-scan images. The subfoveal choroidal thickness was manually measured with image processing software (Fiji[21]) for all eyes.

RESULTS

In control eyes, the standard OCT B-scan images showed the location of the choroid and RPE but did not provide information about the distribution of melanin (Fig. 1E). En face images, including CF, NIR, NIR-AF, and SW-AF, did not provide isolated information about the choroidal melanin (Figs. 1A–D). In contrast, when the PS-OCT data were plotted as pseudocolors in cross-sectional images of DOPU, there were focal color changes that emphasized depolarization consistent with melanin at the RPE and choroid (Fig. 1F). The choroidal melanin location was then determined with the composite DOPU B-scan OCT images (Fig. 1G).

According to subjective evaluation of CF images for the VKH group, 16 eyes from eight patients (seven males, one female; age range, 44–81 years; mean age, 60.1 years) were grouped into the sunset group and 12 eyes from six participants (one male, five females; age range, 39–82 years; mean age, 61.5 years) were grouped into the non-sunset group. Standard OCT B-scan images did not show clear differences between the sunset and non-sunset groups (Figs. 2E, 3E). DOPU B-scan OCT images clearly showed the absence of choroidal melanin in eyes from the sunset group (Figs. 2F, 2G) and the presence of choroidal melanin in the non-sunset group (Figs. 3F, 3G). There was no apparent difference in background reflectance in the NIR, NIR-AF, or SW-AF images between the sunset and non-sunset groups (Figs. 2B–D, 3B–D). Regarding the subjective evaluation by the graders, the concordance

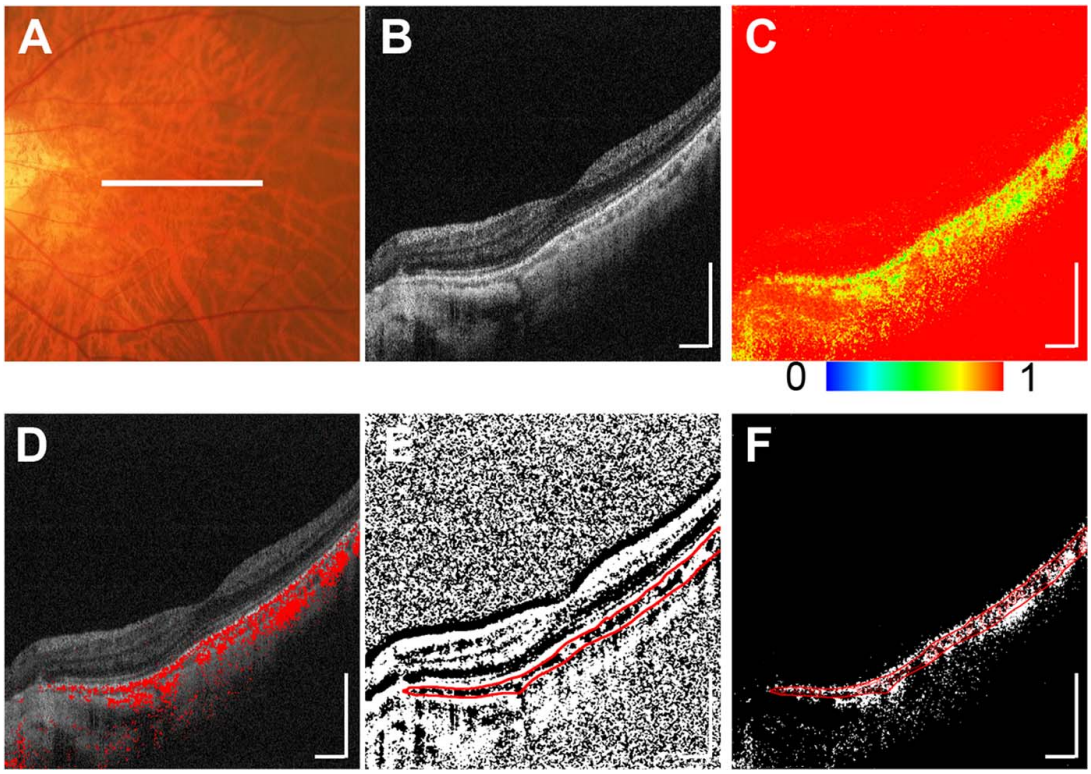

FIGURE 4. PS-OCT imaging from the left eye of a 60-year-old female from the tessellated fundus group. The *white line* in the CF image (**A**) indicates the scan line of the PS-OCT B-scan image (**B**–**F**). The standard OCT B-scan image (**B**) shows choroidal thinning. The DOPU B-scan image (**C**) and composite DOPU B-scan OCT image (**D**) show the presence of choroidal melanin. The *red lines* in the binary image indicate the segmentation line of the choroid (**E**). The *red lines* in the B-scan image for the calculation of the percentage area of low DOPU (**F**) show the boundary of the choroidal interstitial stroma. The *scale bar* in B-scan images represents 500 μm × 500 μm.

percentages (κ values) with the CF images were 0.220, 0.145, and 0.037 for NIR, NIR-AF, and SW-AF images, respectively. The κ values of interobserver agreement (RT, TA) were 1.000, 1.000, 0.364, and 1.000 for the CF, NIR, NIR-AF, and SW-AF images, respectively. In eyes of the tessellated fundus group, CF images with tessellated fundus appearance showed a bright orange background color, similar to the SGF appearance (Fig. 4A). Standard B-scan OCT images showed choroidal thinning (Fig. 4B), and composite DOPU B-scan OCT images clearly showed the presence of melanin in the choroid (Fig. 4D).

Area percentages of low DOPU in the choroidal interstitial stroma (mean ± SD [range]) were 0.005 ± 0.004 (0.0002–0.014), 0.303 ± 0.139 (0.091–0.576), 0.327 ± 0.153 (0.113–0.573), and 0.254 ± 0.136 (0.108–0.598) for the sunset, non-

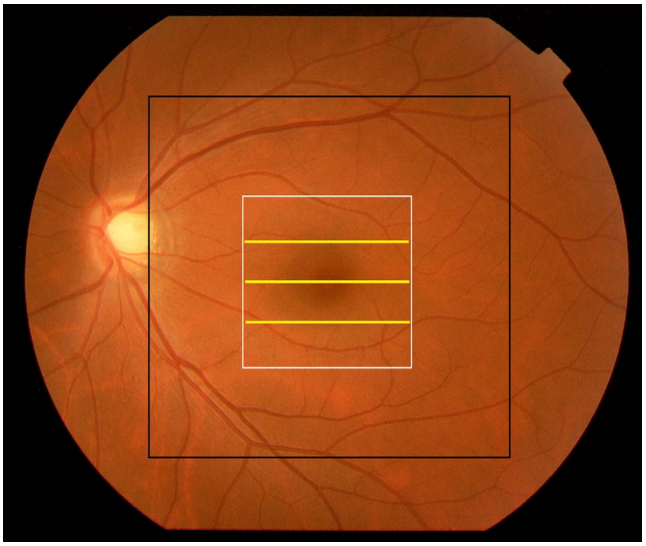

FIGURE 5. Measurement area in a CF image of the left eye of case 6. The *black line* designates the area for subjective evaluation (30° × 30°). The *white line* designates the area for the SGI measurement (300 × 300 pixels). The *yellow lines* designate the scan lines of the PS-OCT B-scan images for the measurement of the percentage area of low DOPU.

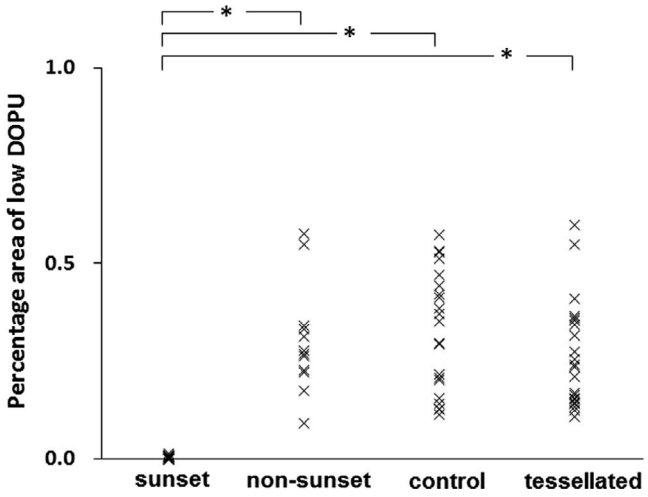

FIGURE 6. The distribution of percentage areas of low DOPU in the choroidal interstitial stroma in the sunset, non-sunset, control, and tessellated fundus groups. *$P < 0.001$.

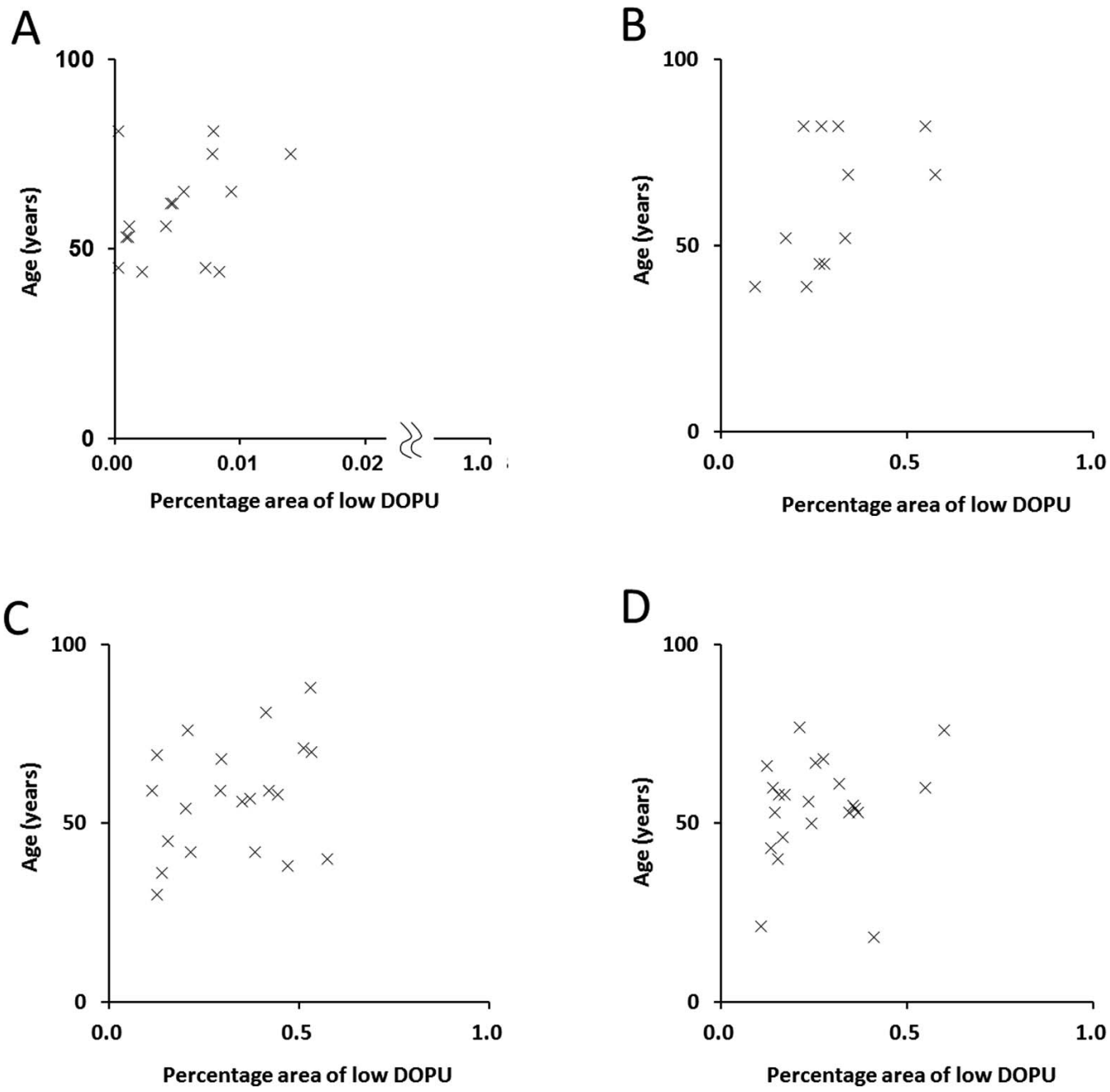

FIGURE 7. Scatterplots illustrating the relationship between the age of the subjects and the mean percentage area of low DOPU in the sunset (**A**), non-sunset (**B**), control (**C**), and tessellated fundus (**D**) groups.

sunset, control, and tessellated fundus groups, respectively. The mean percentage area of low DOPU in the sunset group was significantly lower than that of the other groups ($P < 0.001$; Kruskal-Wallis test; Mann-Whitney U test) and showed no overlap with the other groups (Fig. 6). The coefficient of variation using four repeated measurements (mean ± SD) was 0.16 ± 0.04. The percentage areas of low DOPU did not show significant correlations with age for any of the groups ($R^2 = 0.12$, $P = 0.19$ for the sunset group; $R^2 = 0.24$, $P = 0.10$ for the non-sunset group; $R^2 = 0.09$, $P = 0.20$ for the control group; $R^2 = 0.04$, $P = 0.35$ for the tessellated fundus group; Pearson's correlation; Fig. 7).

The SGI (mean ± SD [range]) in the CF images was 0.649 ± 0.049 (0.565–0.723), 0.578 ± 0.046 (0.500–0.637), 0.550 ± 0.043 (0.465–0.645), and 0.641 ± 0.038 (0.561–0.706) in the sunset, non-sunset, control, and tessellated fundus groups, respectively. The mean SGI in the sunset and tessellated fundus groups was significantly larger than that of the other groups ($P = 0.022$ for sunset and $P < 0.001$ for tessellated fundus; Kruskal-Wallis test; Mann-Whitney U test). The distribution of the SGI in the sunset group substantially overlapped with the other groups (Fig. 8A). In the eyes with VKH disease, the SGI did show a significant negative correlation with the percentage areas of low DOPU for both the sunset and non-sunset group ($R^2 = 0.21$, $P = 0.043$ for the sunset group; $R^2 = 0.34$, $P = 0.045$ for the non-sunset group; Pearson's correlation; Fig. 9).

Subfoveal choroidal thicknesses (mean ± SD [range]) were 172 ± 78 μm (22–328), 256 ± 70 μm (140–346), 237 ± 76 μm (108–385), and 48 ± 19 μm (21–86) for the sunset, non-sunset, control, and tessellated fundus groups, respectively. The mean

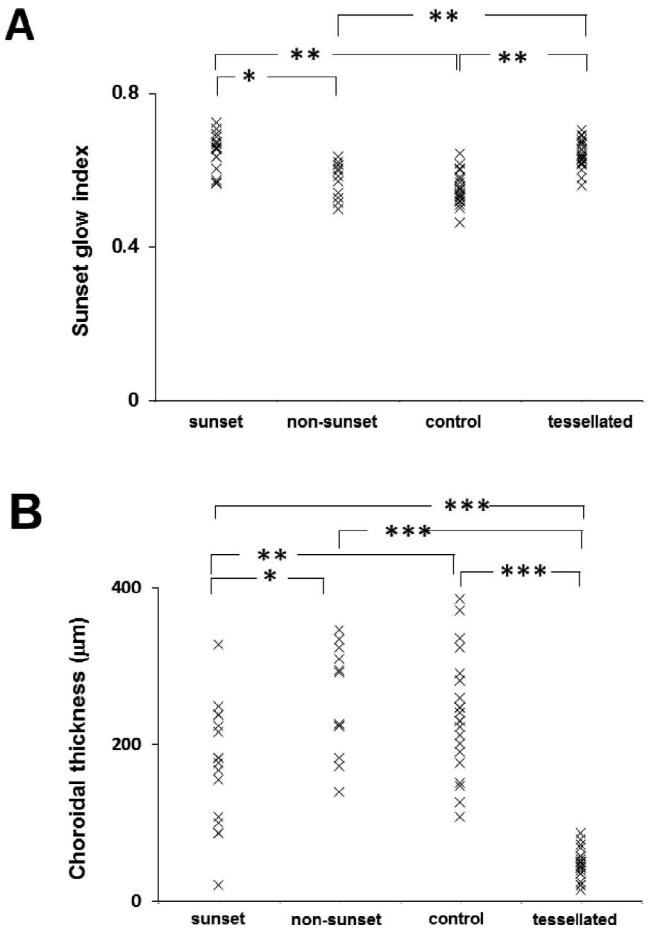

FIGURE 8. (**A**) The distribution of the sunset glow index in the sunset, non-sunset, control, and tessellated fundus groups. $^{*}P = 0.022$, $^{**}P < 0.001$. (**B**) The distribution of subfoveal choroidal thickness in the sunset, non-sunset, control, and tessellated fundus groups. $^{*}P = 0.015$, $^{**}P = 0.022$, $^{***}P < 0.001$

subfoveal choroidal thickness in the tessellated fundus group was significantly smaller than that of the other groups ($P < 0.001$; Kruskal-Wallis test; Mann-Whitney U test). The mean subfoveal choroidal thickness in the sunset group was significantly smaller than that of the non-sunset or control groups ($P = 0.022$; Kruskal-Wallis test; Mann-Whitney U test). The distribution of the subfoveal choroidal thickness in the sunset group substantially overlapped with the other groups (Fig. 8B). In the VKH group, the subfoveal choroidal thickness did not show a significant correlation with the percentage area of low DOPU for either the sunset or non-sunset groups ($R^2 = 0.004$, $P = 0.82$ for the sunset group; $R^2 = 0.13$, $P = 0.13$ for the non-sunset group; Pearson's correlation; Fig. 10).

DISCUSSION

Despite the importance of the SGF appearance for the diagnosis of chronic VKH disease,[4] there are no established objective methods to confirm its existence. In the present study, the disappearance of choroidal melanin in eyes with an SGF was confirmed with PS-OCT. Other imaging modalities, including standard OCT, NIR, NIR-AF, or SW-AF, were not useful in providing specific findings to support the SGF changes.

In normal chorioretinal tissue, melanin is found in RPE cells and choroidal melanocytes.[24] In this study, DOPU B-scan images in control eyes clearly showed the presence of melanin in both the RPE and choroid. In contrast, eyes with an SGF showed the disappearance of choroidal melanin and the preservation of RPE melanin. Histopathologic studies of the SGF show the disappearance of choroidal melanocytes with mild inflammatory cell infiltration, with relative sparing of the overlying RPE.[2,3] In vivo PS-OCT findings confirmed these histopathologic changes.

Suzuki[7] has suggested the use of the SGI for the objective evaluation of color balance in CF images, and an increase in the SGI suggested aggravation of the SGF. In the present study, the percentage area of low DOPU in VKH disease showed a negative correlation with the SGI. Using PS-OCT, the low DOPU in the choroid was thought to result from depolarization of melanin particles.[14] Hence, the percentage area of the low

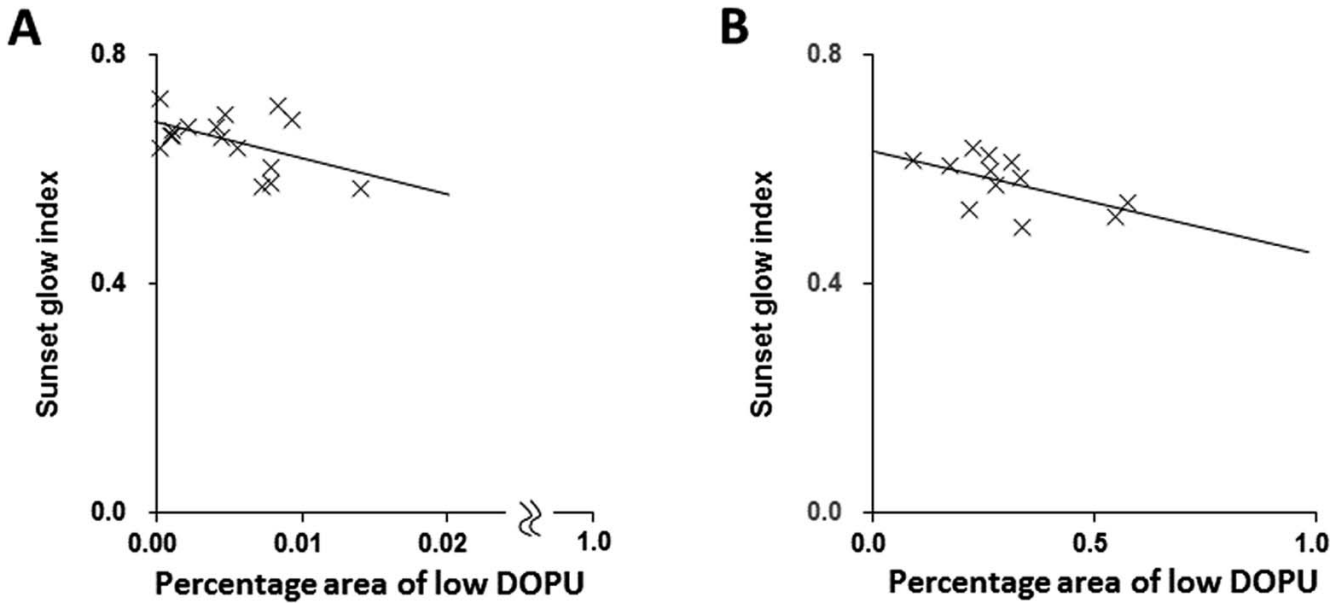

FIGURE 9. Scatterplots of the sunset glow index and mean percentage area of low DOPU in the sunset (**A**) and non-sunset (**B**) groups. *Black lines* show the regression line of the correlation in the sunset (**A**) and non-sunset (**B**) groups.

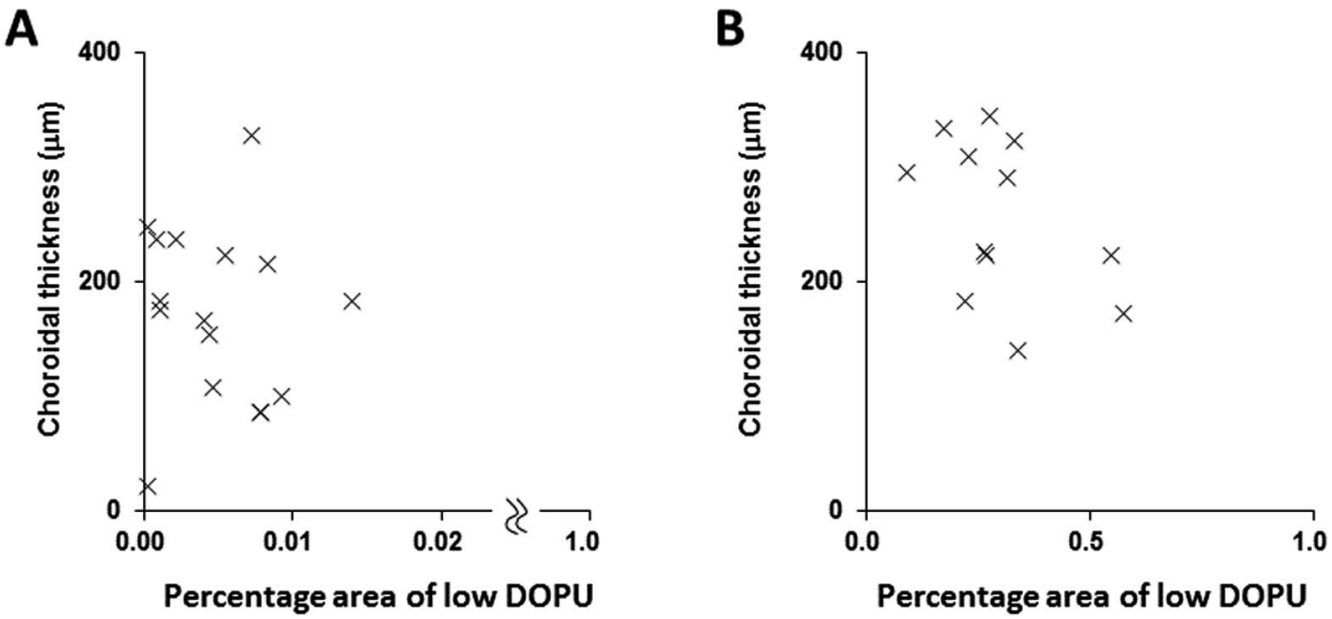

FIGURE 10. Scatterplots of the subfoveal choroidal thickness and mean percentage area of low DOPU in the sunset (**A**) and non-sunset (**B**) groups.

DOPU in the choroidal interstitial stroma could be used as an objective index of choroidal melanin. The correlation of the percentage area of low DOPU with the SGI in the VKH group suggested that PS-OCT measurements can be used as an objective parameter for the development of the SGF. However, the discriminatory ability of the SGI was lower than that of PS-OCT imaging and involved a substantial overlap between the sunset group and other groups. Consistency of color balance is frequently affected by sensor characteristics, spatial resolution, file compression, color management, exposure, saturation, contrast, or a lack of universal standards.[25,26] The retina presents a narrow color gamut, compared with most other scenes, and the red color channel might be frequently saturated.[25] Standardization of these parameters is therefore necessary for the objective evaluation of the CF images. Furthermore, the influence of RPE melanin might impair the evaluation of choroidal melanin with CF images. In contrast, DOPU B-scan images could be evaluated solely with choroidal melanin, without the interference of RPE melanin. Hence, PS-OCT imaging might be more reliable than CF imaging to evaluate the SGF.

In this study, NIR, SW-AF, or NIR-AF did not show specific findings for the SGF. Low concordance of these images with the CF images showed a limited ability to evaluate the SGF. AF in SW-AF imaging is thought to originate from lipofuscin in the RPE.[27] Our study supported the insensitive nature of SW-AF imaging for choroidal melanin. AF in NIR-AF is thought to originate from melanin in the RPE or choroidal melanocytes, or melanin-containing inflammatory cells.[28] In SGF, AF in NIR-AF imaging might be decreased by the disappearance of choroidal melanocytes. However, in this study, subjective evaluation with NIR-AF showed substantial inconsistencies with the CF or PS-OCT. One possible explanation is the relative sparing of melanin in the RPE, which might conceal the AF signal from the choroid. Another possibility is the difficulty in confirming diffuse changes in the background AF because of a lack of reference values in NIR-AF imaging. Further studies with objective measurement of NIR-AF signals might be a possible solution for these limitations.

In this study, subfoveal choroidal thickness decreased significantly in the sunset group compared to the non-sunset group. In the sunset group, chronic inflammation might have induced tissue necrosis, fibrosis, and finally, choroidal thinning.[2,3] However, the discriminatory ability of SGF was limited by substantial overlap with control or non-sunset groups. Moreover, choroidal thickness did not show a significant correlation with the PS-OCT. The distribution of normal choroidal thickness was highly diverse compared to other retinal OCT parameters, such as retinal thickness.[29] Furthermore, there might be variations in the severities of choroidal thickness reductions in an SGF. These factors might impede the ability of choroidal thickness measurements to evaluate the SGF. However, choroidal thickness in the tessellated fundus group was significantly thinner than that of the sunset group. DOPU B-scan OCT images in the tessellated fundus group represented the retention of melanocytes despite choroidal thinning. These findings indicated that the bright fundus color in a tessellated fundus originates from the choroidal thinning, not melanin disappearance.

This study had some limitations. With the relatively small number of patients, our study evaluated only some aspects of sunset glow appearance. To evaluate the development of the SGF, a long-term observational study from the onset of the intraocular inflammation is required. It should also be noted that choroidal melanin content is affected by ethnic differences.[30] Given that this study only evaluated Japanese patients, future research projects should investigate whether our findings extend to other ethnicities. Although a previous histologic study has indicated that human choroidal melanin tends to decrease with age,[30] we did not observe in the present study any significant correlation between the percentage area of low DOPU and age in any of the groups. Furthermore, although there is evidence that a monotonic relationship exists between DOPU and melanin,[14] the nature of this relationship remains poorly understood and is seldom investigated. Larger cohort studies are required to thoroughly evaluate the impact of age on DOPU and melanin.

In conclusion, this study showed the clinical usefulness of PS-OCT to evaluate the SGF in VKH disease. DOPU measurement with PS-OCT could noninvasively evaluate choroidal melanin content and may have the potential for the clinical assessment of chronic VKH disease. However, PS-OCT is not

yet commercially available for widespread use and maintenance and operation of PS-OCT systems is more complicated than for commercialized standard OCT. Further study is necessary to confirm the possible use of PS-OCT for chronic VKH disease.

Acknowledgments

Supported in part by KAKENHI (15K10905, 16K11330, 15K13371) and the Japanese Ministry of Education, Culture, Sports, Science and Technology (MEXT) through a contract with the Regional Innovation Ecosystem Development Program.

Disclosure: **M. Miura**, None; **S. Makita**, None; **Y. Yasuno**, None; **R. Tsukahara**, None; **Y. Usui**, None; **N.A. Rao**, None; **Y. Ikuno**, None; **S. Uematsu**, None; **T. Agawa**, None; **T. Iwasaki**, None; **H. Goto**, None

References

1. O'Keefe GA, Rao NA. Vogt-Koyanagi-Harada disease. *Surv Ophthalmol*. 2017;62:1–25.
2. Inomata H, Sakamoto T. Immunohistochemical studies of Vogt-Koyanagi-Harada disease with sunset sky fundus. *Curr Eye Res*. 1990;9(suppl):35–40.
3. Rao NA. Pathology of Vogt-Koyanagi-Harada disease. *Int Ophthalmol*. 2007;27:81–85.
4. Read RW, Holland GN, Rao NA, et al. Revised diagnostic criteria for Vogt-Koyanagi-Harada disease: report of an international committee on nomenclature. *Am J Ophthalmol*. 2001;131:647–652.
5. Keino H, Goto H, Usui M. Sunset glow fundus in Vogt-Koyanagi-Harada disease with or without chronic ocular inflammation. *Graefes Arch Clin Exp Ophthalmol*. 2002; 240:878–882.
6. Keino H, Goto H, Mori H, Iwasaki T, Usui M. Association between severity of inflammation in CNS and development of sunset glow fundus in Vogt-Koyanagi-Harada disease. *Am J Ophthalmol*. 2006;141:1140–1142.
7. Suzuki S. Quantitative evaluation of "sunset glow" fundus in Vogt-Koyanagi-Harada disease. *Jpn J Ophthalmol*. 1999;43: 327–333.
8. Okada AA, Mizusawa T, Sakai J, Usui M. Videofunduscopy and videoangiography using the scanning laser ophthalmoscope in Vogt-Koyanagi-Harada syndrome. *Br J Ophthalmol*. 1998; 82:1175–1181.
9. Rao NA, Gupta A, Dustin L, et al. Frequency of distinguishing clinical features in Vogt-Koyanagi-Harada disease. *Ophthalmology*. 2010;117:591–599.
10. Lee EK, Lee SY, Yu HG. A clinical grading system based on ultra-wide field retinal imaging for sunset glow fundus in Vogt-Koyanagi-Harada disease. *Graefes Arch Clin Exp Ophthalmol*. 2015;253:359–368.
11. Nakai K, Gomi F, Ikuno Y, et al. Choroidal observations in Vogt-Koyanagi-Harada disease using high-penetration optical coherence tomography. *Graefes Arch Clin Exp Ophthalmol*. 2012;250:1089–1095.
12. Takahashi H, Takase H, Ishizuka A, et al. Choroidal thickness in convalescent Vogt-Koyanagi-Harada disease. *Retina*. 2014; 34:775–780.
13. Pircher M, Hitzenberger CK, Schmidt-Erfurth U. Polarization sensitive optical coherence tomography in the human eye. *Prog Retin Eye Res*. 2011;30:431–451.
14. Baumann B, Baumann SO, Konegger T, et al. Polarization sensitive optical coherence tomography of melanin provides intrinsic contrast based on depolarization. *Biomed Opt Express*. 2012;3:1670–1683.
15. Baumann B, Schirmer J, Rauscher S, et al. Melanin pigmentation in rat eyes: in vivo imaging by polarization-sensitive optical coherence tomography and comparison to histology. *Invest Ophthalmol Vis Sci*. 2015;56:7462–7472.
16. Miura M, Yamanari M, Iwasaki T, et al. Imaging polarimetry in age-related macular degeneration. *Invest Ophthalmol Vis Sci*. 2008;49:2661–2667.
17. Sugiyama S, Hong YJ, Kasaragod D, et al. Birefringence imaging of posterior eye by multi-functional Jones matrix optical coherence tomography. *Biomed Opt Express*. 2015;6: 4951–4974.
18. Hong YJ, Miura M, Ju MJ, Makita S, Iwasaki T, Yasuno Y. Simultaneous investigation of vascular and retinal pigment epithelial pathologies of exudative macular diseases by multifunctional optical coherence tomography. *Invest Ophthalmol Vis Sci*. 2014;55:5016–5031.
19. Gotzinger E, Pircher M, Geitzenauer W, et al. Retinal pigment epithelium segmentation by polarization sensitive optical coherence tomography. *Opt Express*. 2008;16:16410–16422.
20. Makita S, Hong YJ, Miura M, Yasuno Y. Degree of polarization uniformity with high noise immunity using polarization-sensitive optical coherence tomography. *Opt Lett*. 2014;39: 6783–6786.
21. Schindelin J, Arganda-Carreras I, Frise E, et al. Fiji: an open-source platform for biological-image analysis. *Nat Methods*. 2012;9:676–682.
22. Neelam K, Chew RY, Kwan MH, Yip CC, Au Eong KG. Quantitative analysis of myopic chorioretinal degeneration using a novel computer software program. *Int Ophthalmol*. 2012;32:203–209.
23. Yoshihara N, Yamashita T, Ohno-Matsui K, Sakamoto T. Objective analyses of tessellated fundi and significant correlation between degree of tessellation and choroidal thickness in healthy eyes. *PLoS One*. 2014;9:e103586.
24. Hu DN, Simon JD, Sarna T. Role of ocular melanin in ophthalmic physiology and pathology. *Photochem Photobiol*. 2008;84:639–644.
25. Hubbard LD, Danis RP, Neider MW, et al. Brightness, contrast, and color balance of digital versus film retinal images in the Age-Related Eye Disease Study 2. *Invest Ophthalmol Vis Sci*. 2008;49:3269–3282.
26. Veiga D, Pereira C, Ferreira M, Goncalves L, Monteiro J. Quality evaluation of digital fundus images through combined measures. *J Med Imaging*. 2014;1:014001.
27. Delori FC, Dorey CK, Staurenghi G, Arend O, Goger DG, Weiter JJ. In vivo fluorescence of the ocular fundus exhibits retinal pigment epithelium lipofuscin characteristics. *Invest Ophthalmol Vis Sci*. 1995;36:718–729.
28. Keilhauer CN, Delori FC. Near-infrared autofluorescence imaging of the fundus: visualization of ocular melanin. *Invest Ophthalmol Vis Sci*. 2006;47:3556–3564.
29. Agawa T, Miura M, Ikuno Y, et al. Choroidal thickness measurement in healthy Japanese subjects by three-dimensional high-penetration optical coherence tomography. *Graefes Arch Clin Exp Ophthalmol*. 2011;249:1485–1492.
30. Weiter JJ, Delori FC, Wing GL, Fitch KA. Retinal pigment epithelial lipofuscin and melanin and choroidal melanin in human eyes. *Invest Ophthalmol Vis Sci*. 1986;27:145–152.

Investigative Ophthalmology & Visual Science